

Creating and coupling a high-resolution DTM with a 1-D hydraulic model in a GIS for scenario-based assessment of avulsion hazard in a gravel-bed river

G.R. Aggett^{a,*}, J.P. Wilson^b

^a AMEC Earth and Environmental, 1002 Walnut Street, Boulder, CO 80302, USA

^b Department of Geography, University of Southern California, Los Angeles, CA 90089-0255, USA

ARTICLE INFO

Article history:

Received 4 July 2008

Received in revised form 28 March 2009

Accepted 9 June 2009

Available online 26 July 2009

Keywords:

Avulsion hazard

Streampower

GIS

LIDAR

HEC-RAS

ABSTRACT

In this paper we explore the development and assimilation of a high resolution topographic surface with a one-dimensional hydraulic model for investigation of avulsion hazard potential on a gravel-bed river. A detailed channel and floodplain digital terrain model (DTM) is created to define the geometry parameter required by the 1D hydraulic model HEC-RAS. The ability to extract dense and optimally located cross-sections is presented as a means to optimize HEC-RAS performance. A number of flood scenarios are then run in HEC-RAS to determine the inundation potential of modeled events, the post-processed output of which facilitates calculation of spatially explicit shear stress (τ) and level of geomorphic work (specific stream power per unit bed area, ω) for each of these. Further enhancing this scenario-based approach, the DTM is modified to simulate a large woody debris (LWD) jam and active-channel sediment aggradation to assess impact on inundation, τ , and ω , under previously modeled flow conditions. The high resolution DTM facilitates overlay and evaluation of modeled scenario results in a spatially explicit context containing considerable detail of hydrogeomorphic and other features influencing hydraulics (bars, secondary and scour channels, levees). This offers advantages for: (i) assessing the avulsion hazard potential and spatial distribution of other hydrologic and fluvial geomorphic processes; and (ii) exploration of the potential impacts of specific management strategies on the channel, including river restoration activities.

© 2009 Elsevier B.V. All rights reserved.

1. Introduction

A legacy of glaciation and forested land cover strongly influences river dynamics in Washington State (WA) (Montgomery and Buffington, 1993). For example, several recent studies have revealed that accumulations of large woody debris (LWD) have historically been significant, and perhaps dominant channel altering mechanisms, and continue to directly influence channel avulsions (e.g. Abbe and Montgomery, 2003; O'Connor et al., 2003). In general we can expect avulsion frequency to increase with increasing deposition rate in the channel (Bryant et al., 1995; Mackey and Bridge, 1995; Heller and Paola, 1996). In the Pacific Northwest the downstream sedimentation impacts of dam removal are an ongoing management concern (e.g. Lorang and Aggett, 2005), and a major influence on channel avulsion. Aggradation following dam removal raises bed elevation, enhances inundation and thus increases avulsion potential during floods.

Avulsion processes in gravel-bed rivers are typically manifested as large-scale switching of primary channel flow as hydraulic conditions allow the river to migrate across the floodplain to preferred gradients, frequently provided by secondary and abandoned channels. This

process can occur rapidly in flood conditions, especially if the required high water levels are achieved by downstream damming caused by snagging and build up of LWD assemblages and/or rapid aggradation of sediment. Such channel migration poses a considerable threat to property and infrastructure and has come under increasing scrutiny from the WA Departments of Ecology and Transportation, who recently produced detailed guidelines for assessing and delineating channel migration zones (CMZs) (Rapp and Abbe, 2003). The methodology is characterized by the following equation which itself is the cumulative product of historical analysis and field interpretations:

$$\text{CMZ} = \text{HMZ} + \text{AHZ} + \text{EHA} - \text{DMA} \quad (1)$$

where HMZ is the Historical Migration Zone – the collective area the channel occupied in the historical record; AHZ is the Avulsion Hazard Zone – the area at risk of avulsion over the timeline of the CMZ; EHA is the Erosion Hazard Area – the area not included in the HMZ or AHZ that is at risk of bank erosion from stream flow or mass wasting over the timeline of the CMZ; DMA is the disconnected migration area.

The avulsion hazard zone (AHZ) is the most dynamic component of this equation and must be reliably delineated if the CMZ mapping process is to provide adequate locational information for hazard mitigation. However, while focused and detailed fieldwork at the

* Corresponding author.

E-mail address: graeme.aggett@amec.com (G.R. Aggett).

reach scale can reveal the location and nature of past and potential avulsion sites (e.g. Abbe and Montgomery, 2003), resources for this level of investigation are rarely available for study of a larger system. Rather, the geomorphologist is likely to be constrained to an initial reconnaissance determining the nature of the channel and floodplain, supported by analysis of historical and contemporary aerial photographs and other imagery. While it has little predictive power, this historical approach is a direct and convincing method for documenting past changes, and within a GIS setting provides a solid framework with which to test and analyze hypotheses of the spatial and temporal variability of channel response to changing water, sediment and LWD inputs (e.g. Gurnell and Montgomery, 1998; Leys and Werrity, 1999) and to determine historical locales of avulsion which, depending on prevailing floodplain condition and processes, are used as indicators of future avulsion sites. However, even when combined with high resolution image and digital terrain model (DTM) analysis, such avulsion sites are difficult to determine with certainty. Once potential AHZs have been identified, considerable judgment is required to determine the route inundation flows are likely to take outside of the main channel, and whether or not the flow has the potential to do the geomorphic work required to carve a new channel or reactivate an old one.

Given the importance of the AHZ in the CMZ mapping process, the aim of this research is to develop an approach that can generate more quantitative, spatially explicit information to increase the reliability of AHZ delineation. Based on a Light Detection And Ranging (LiDAR) DTM (Aggett, 2005) and the widely used model HEC-RAS, the detailed topographic representation of the channel is shown to allow for scenario-based hydraulic modeling that can assess inundation under a range of probable flow conditions, and in response to a number of avulsion forming processes (e.g. LWD damming; bed aggradation). This enhances our understanding of potential channel migration in response to changing environmental conditions by providing a better spatial understanding of the location and degree of geomorphic work likely to be done.

While the concept of geomorphic work is difficult to define precisely (Costa and O'Connor, 1995), straightforward measures of fluvial energy such as stream power can be most useful for defining the domains of particular types of channel response to individual floods (Rhoads, 1987; Miller, 1991; Knighton, 1999). The geomorphic effectiveness of flows is linked to specific stream power, which is a function of flow magnitude, channel dimensions, and energy gradient (Baker and Costa, 1987)

$$\tau = \gamma RS \quad (2)$$

$$\omega = \tau v = \gamma QS / w \quad (3)$$

where ω is stream power per unit boundary area in $W m^{-2}$, τ is boundary shear stress in $N m^{-2}$, γ is the specific weight of clear water ($9800 N m^{-3}$), Q is discharge in $m^3 s^{-1}$, S is energy slope, w is flow width in m, R is the hydraulic radius of water in m, and v is the mean flow velocity in $m s^{-1}$. Some measurement or estimate of channel and/or floodplain slope (for overbank flows), and potential water depth for a flow are required to estimate shear stress. The increasing availability of digital terrain information and terrain modeling tools in GIS has enabled several researchers to utilize DTMs to investigate the spatial variability of stream power throughout river systems. However, as Finlayson and Montgomery (2004) point out, early enthusiasm for GIS-based geomorphic analysis was dampened by the sobering reality that hydrologic modeling using DTMs is strongly affected by coarse grid-sizes that cannot resolve fine-scale landscape features. This is especially true for rivers where until recently DTMs have not typically been available at the channel scale unless created for specific research objectives using photogrammetry or detailed field survey using total station (e.g. Lane et al., 1993, 1994; Lane, 1998; Westaway et al., 2000; Fuller et al., 2003). More widely available DTMs of 10 m or greater resolution do not contain hydraulic details of

the channel itself, and certainly not secondary and abandoned channels, swales, ponds and backwater channels, that may be hydraulically influential on avulsion processes.

2. Tools for scenario-based assessment of inundation and stream power

2.1. Hydraulic modeling

New data sources such as LiDAR are enabling the creation of DTMs with elevation precision in the range ± 0.5 m (Lane and Chandler, 2003), and the ability to collect synoptic yet dense elevation points has facilitated topographic parameterization of hydraulic model studies of reaches up to 60 km long (e.g. Marks and Bates, 2000; Horritt and Bates, 2002). River systems are highly heterogenous so it seems intuitive that increased spatial resolution will improve the realism of a model's predictive ability. However, recent research has shown that complex 2D models based on high resolution grids do not necessarily show expected improvements in solution stability as grid size moves closer to the scale of processes under investigation, nor show results closer to those measured in the field or validated by remote sensing (e.g. Bates et al., 1998; Hardy et al., 1999; Marks and Bates, 2000; Bates et al., 2003). Additionally, while high resolution models are potentially more realistic they are also more complex and require more expensive parameterization to work effectively, making 2D modeling beyond the resources of many river researchers. Less complicated alternatives are 1D models based on the St. Venant shallow water equations, including the widely used river engineering model, HEC-RAS. Its relative ease of use makes HEC-RAS an appropriate choice for our avulsion hazard modeling approach. The system has the ability to quite rapidly compute water surface profiles for several different characterizations of the system under study. Modifications can be made to channel geometry and flow data, and 'plans' formulated by selecting a particular geometry and/or flow file enabling comparisons between existing and future channel and flow conditions to be made. Secondly, optional capabilities in HEC-RAS allow for mixed flow regime calculations, and flow distribution calculations via segmentation of the cross-section in left and right overbank 'slices', based on geometric, hydraulic and roughness characteristics.

While HEC-RAS development has been primarily focused on the requirements of river engineers, its capabilities have been put to good use by fluvial geomorphologists (e.g. Springer et al., 2003; Wilkinson et al., 2004). However, these geomorphic investigations have typically been constrained to tabular and one-dimensional graphical output and the limitation this places on interpretation and analyses. The recent development of HEC-GeoRAS, a GIS-based pre- and post-processor for parameterizing HEC-RAS with channel geometry, roughness and other hydraulic parameters has improved this situation considerably (Maidment, 2002). GeoRAS can also handle output data created by HEC-RAS, allowing import of predicted 2D water surfaces and velocity information back to GIS for visualization and analysis.

2.2. Terrain modeling of the channel

Traditionally, HEC-RAS channel geometry is defined by field surveyed cross-sections indexed by river station, data that are often necessarily spaced a considerable distance apart. More recently, the availability of digital topographic data (e.g. the 7.5-minute and 15-minute digital elevation products of the USGS's National Elevation Dataset program) has enabled floodplain geometry to be extracted from these digital datasets, though these typically do not characterize channel geometry in any detail. A dense LiDAR-based DTM presents opportunities to cut cross-sections at optimal locations and with close spacing, shifting the modeling approach at least conceptually towards a model set-up that is more spatially distributed in nature, and with a subsequent expectation of enhanced model performance. Given this, it is also reasonable to expect that misrepresentation of

topography in high resolution DTMs could cause similarly high levels of error propagation and spurious model performance (e.g. [Nicholas and Walling, 1998](#)). Several studies have considered HEC-RAS performance when LiDAR data are available for defining channel geometry, and issues associated with creation of a LiDAR-based DTM for this task (e.g. [Omer et al., 2003](#); [Wang and Zheng, 2005](#)). Careful surface model construction, enhancements, and error assessment are required for both 2D and 1D hydraulic modeling applications (e.g. [Wise, 1998](#); [French, 2003](#); [Lane et al., 2004](#)) and recent studies have begun to investigate the influence of LiDAR idiosyncrasies on model output. For example, [Gueudet et al. \(2004\)](#) investigate the influence of post-spacing density of a LiDAR-derived DTM on HEC-RAS predicted flood surfaces. The desire to selectively thin dense LiDAR datasets to reduce data volume highlights a related data quality issue raised by [Lane and Chandler \(2003\)](#), that the advantages of automated data collection for river studies is also its nemesis – the volume of data generated means that the proportion of check data that can be used to assess error is reduced to the point of becoming unreliable. [Charlton et al. \(2003\)](#) use detailed ground survey cross-sections and compared these with those cut from LiDAR to assess the fidelity of the surface model, this improving on the often-used but potentially misleading global measurement of (root mean square) error which fails to represent the spatial structure of the error field ([Lane, 1998](#)). [Charlton et al. \(2003\)](#) and [Grounds et al. \(2004\)](#) illustrate the 'data gap' in the wetted part of the channel, where many LiDAR sensors do not effectively penetrate water, while [Fowler \(2001\)](#) highlights the need to augment LiDAR data at critical locations. In river modeling this might be at the river bank, where LiDAR footprints fail to fall exactly on the bank edge. Interpolation of LiDAR points to create a terrain surface will fail to create a reliable representation of the bank-river interface, unless heighted breaklines are created and available for the terrain

modeling process. The purpose of this paper is to present a proof of concept for the avulsion-hazard-scenario-modeling approach, so these issues are not discussed in great detail within this paper. Details of how the baseline (i.e. starting) DTM was generated are in [Aggett \(2005\)](#).

Notwithstanding the previous discussion, LiDAR data offer a number of advantages here. The first is that in handling the point clouds representing the elevations of LiDAR footprints it is possible to classify the surface prior to surface generation, to remove points (e.g. vegetation), or add points to simulate LWD damming and aggradation of the channel bed (especially useful given that HEC-RAS is a fixed bed model) opening the door to analyzing multiple hydraulic scenarios (e.g. [Shapiro and Nelson, 2004](#)). Secondly, once constructed, the surface model is overlaid with imagery and rendered interactively in 2.5D providing an opportunity to immerse in a highly realistic virtual field environment that facilitates optimum locating and digitizing of cross-sections for HEC-RAS modeling, based on hydraulic and other critical characteristics of the reach under study. Lastly, the visual and textural information contained in the surface model allows for optimum selection and digital delineation of n values for modeling, an important issue given the reported sensitivity of HEC-RAS to roughness parameters ([Pappenberger et al., 2005](#)).

3. Study area and data

The study area ([Fig. 1](#)) is a 3.2 km section of a highly dynamic 22.5 km gravel-bed reach of the Naches River, which originates in the Cascade Mountains east of Mount Rainier (4392 m) in Washington State, USA.

The River flows through a wide alluvial valley constrained by uplifted basalt fold-belt ridges on either side. Field reconnaissance indicated that the system appears to be aggrading and that chute cutoffs, thalweg and meander shifts and bank erosion are observed ([Aggett,](#)

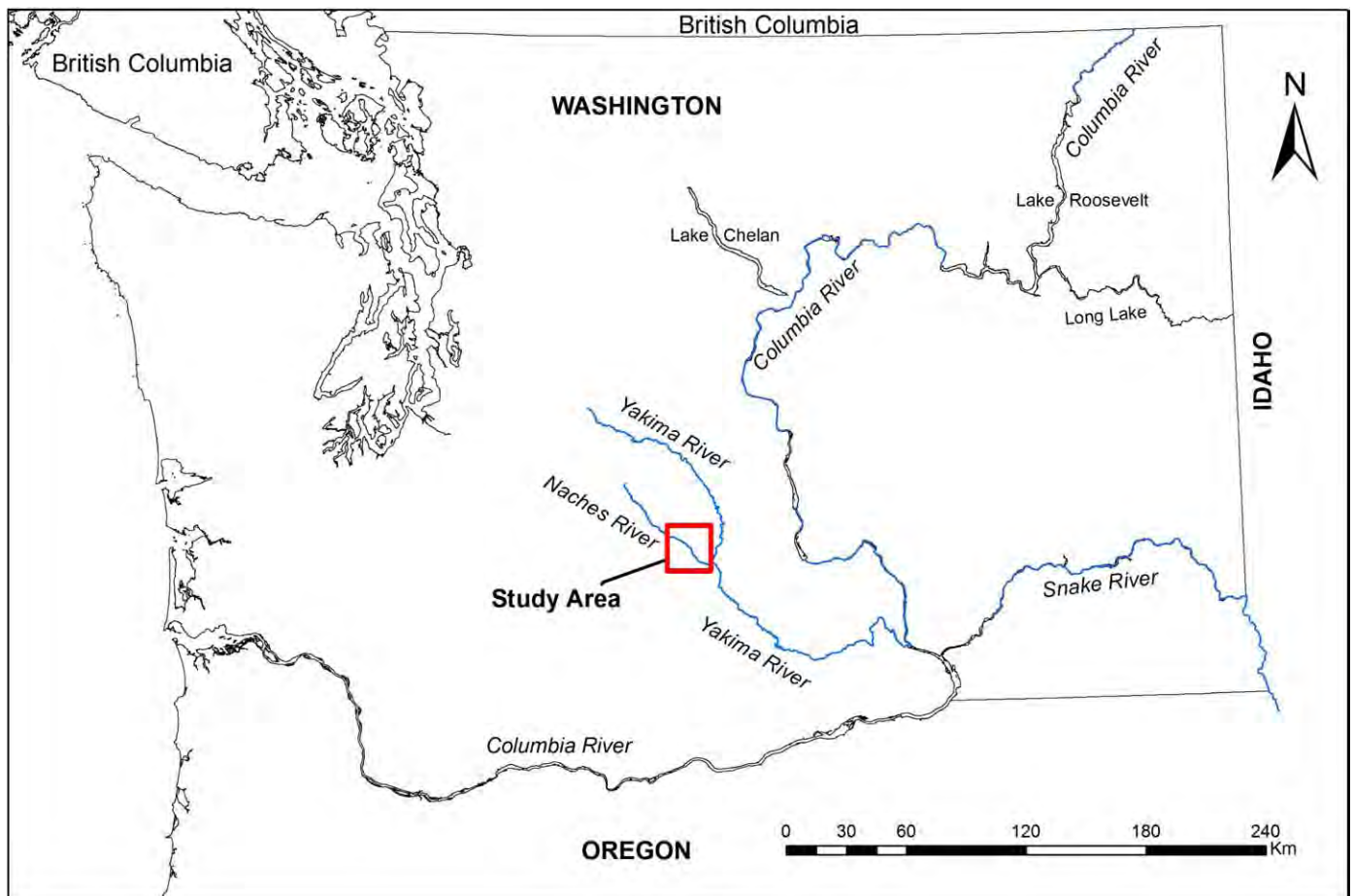


Fig. 1. Location of study area.

2005). Evidence of avulsion such as incision of new and reoccupation of existing channels is clear at several sites, and a major avulsion in the lower study reach was reported to have occurred in a recent (1996) flood. LWD jams and other obstructions have initiated rapid aggradation of gravel in many sections, and are clearly influential in channel migration. Interviews with local people indicated ice-jams and beaver dams are also a problem given their potential to exacerbate flooding in winter and spring (Aggett, 2005). Fig. 2a shows a channel migration zone hazard map for the study reach. Fig. 2b is the study reach at low-flow. A potential avulsion channel is barely visible in this high definition panchromatic image, highlighting the difficulty in establishing the location, severity, and possible outcomes of avulsion using image analysis alone.

Dam regulation of the Naches River results in lower-than-natural flows during the winter months and higher-than-natural flows during the summer months. Flow comes from snowmelt and rainfall on the eastern slopes of the Cascade Mountains and average flows are highest during the months of April, May, and June as a result of spring snowmelt runoff. Peak flood flows typically occur during the winter, however, associated with rain-on-snow events on saturated and frozen soils. The US Army Corps of Engineers (1972) modeled an intermediate flood (100 yr) at $910 \text{ m}^3/\text{s}$, and a 'standard project flood' (reasonable upper limit of flooding on the Naches River) at $2384 \text{ m}^3/\text{s}$. Table 1 presents the largest historic flood events on the Naches River.

LiDAR acquisition for this project was conducted in October 2000 by Horizons Inc. using a AeroScan laser scanner with a 15 kHz pulse rate, 13 Hz sinusoidal scan rate and average swath width of 1225 m. This enabled a post spacing of 3.77 m, absolute horizontal and vertical accuracies being reported at $\pm 40 \text{ cm}$ and $\pm 20 \text{ cm}$ respectively. This sensor can receive up to five returns for every laser pulse, allowing for receipt of return data from multiple objects as the laser beam travels towards the ground. For example, in the riparian zone the beam may hit

the leaves of the Cottonwood canopy (generating return 1), then a branch (return 2), and finally the ground (return 3). This sensor does not penetrate water, though returns from the water surface were found to be consistent enough to interpolate a water surface from which we computed water surface slope. This compared well with one surveyed in the field during the field campaign by placing the total station base on the water surface at multiple locations along the thalweg over two separate 400 m reach lengths. A color infra-red (CIR) digital dataset (30 cm pixels) was co-flown with the LiDAR data in October 2000 by Horizons Inc. Stage at time of flight in October 2000 was 3.69 m and 3.7 m at the end of July 2002. This low flow condition minimized the impact of the subaqueous data gap due to LiDAR limitations. To support a river mapping project Quickbird multispectral data (high spatial resolution satellite imagery with 60 centimeter panchromatic and 2.4 meter multispectral bands) were obtained for the same area and used in combination with LiDAR data, to delineate pools, riffles, glides, lateral and island bars and floodplain gravel, and mature and juvenile (recently disturbed) Cottonwood stands (Aggett, 2005). Color stereo pairs of the River flown at 1:10,000 in 2002 were scanned from original negatives at $12.5 \mu\text{m}$. Ground truthing for this project involved GPS mapping of many of these units in the field. 72 dense cross-sections of the floodplain and river channel were resurveyed with a Leica TC705 total station to compare with 1972 sections surveyed by the US Army Corps of Engineers (1972). This data formed the foundation for validating the LiDAR DTM (Aggett, 2005). Table 2 provides an overview of data used in this study.

4. Methods

4.1. Terrain modeling – surface models (SM) 1 and 2

The raw LiDAR data were manipulated in TerraScan running in the MicroStation CAD environment. TerraScan is different from typical

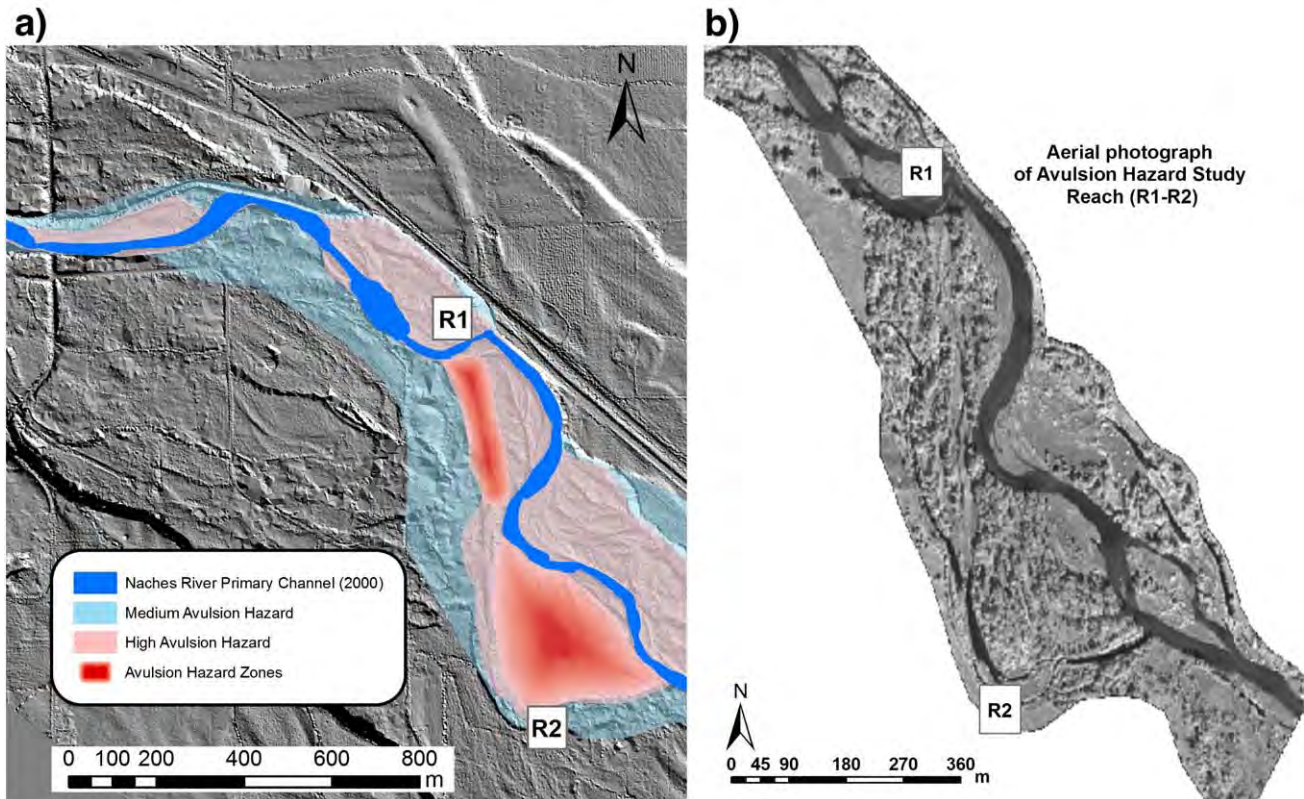


Fig. 2. Channel migration zone hazard map for a reach of the Naches River, WA (2a). (2b) is an aerial photograph of the study reach at low-flow. A relic channel runs between Avulsion Study Reach 1 and 2 (R1–R2), and constitutes a potential avulsion channel which is barely visible in this high definition panchromatic image, highlighting the difficulty in establishing the location, severity, and possible outcomes of avulsion using image analysis alone (from: Aggett, 2005).

Table 1
Largest historic flood events on the Naches River, WA.

Date of crest	Flow (m ³ /s)	Stage ^a (m)	Comments
22-Dec-1933	911.8	6.83	Prompted construction of federal levee system.
9-Feb-1996	592.5	6.82	Largest flood since construction of levees. Natural (unregulated) flow estimated to be 796.5 m ³ /s
24-Nov-1909	549.4	6.0	Several avulsions obvious from aerial photos
2-Dec-1977	509.7	6.13	Little information available. Two flood peaks within 1–1/2 weeks. Water filtration plant shut down because of turbidity.
30-Dec-1917	475.77	5.76	Little information available.
1-Dec-1995	465.4	5.79	Two private bridges destroyed in Nile area. Rattlesnake Creek bridge approach destroyed.
13-Dec-1921	537.0	5.58	Little information available.
4-Dec-1975	399.27	5.61	Highway 12 threatened by channel shifting.
1-Jun-1956	376.61	5.46	No information.
17-Jun-1974	362.45	5.49	City of Yakima's drinking water main damaged.

^a Stage recorded at USBR Gage #1249400, Naches River near Naches.

geospatial handling software (GIS) applications in that it is dedicated to processing, viewing and classifying laser point cloud data. It readily handles millions of points, and is now widely used for processing LiDAR data for earth science applications. The application reads points from XYZ text files, and allows the analyst to define and classify point classes such as ground, vegetation, and water (Fig. 3). Registration and coloring of points in clouds, combined with powerful viewing by section and fly-through in 3D, enables the analyst to iteratively improve point classification and subsequent surface characterization. A critical component of this process is the filtering of ground points to create a 'bare-earth' surface, a classification routine consisting of two phases. First we searched the raw points and built an initial, temporary TIN surface model, the triangles of which are mostly above the ground with only some vertices touching ground. Spurious low points are then separated from 'real' low points in the ground vicinity and removed. In the second phase of classifying ground points, we start to mold the model upwards by iteratively adding new laser points to it. Each added point allows the surface to follow the real ground surface more closely (Fig. 4).

In a similarly iterative process, above ground points primarily representing vegetation are removed to facilitate creation of both a 'vegetated' and a bare-earth surface, the latter suitable for hydrologic and hydraulic modeling. Errors of omission and commission can have strong impacts on misinterpretation of the true ground surface, thus this strong control over point manipulation is thought to be advantageous over vegetation removal algorithms that de-spike surfaces interpolated from raw LiDAR data (e.g. Haugerud et al., 2001), this allowing little user input. Draping of color infra-red image data was used to further enhance the reliability of vegetation removal by further development of an adaptive point removal process developed by Raber et al. (2002).

Once confident with the point classification and definition of 'bare-earth', we took the points into a GIS environment where a terrain modeling database was constructed consisting of bare-earth classified

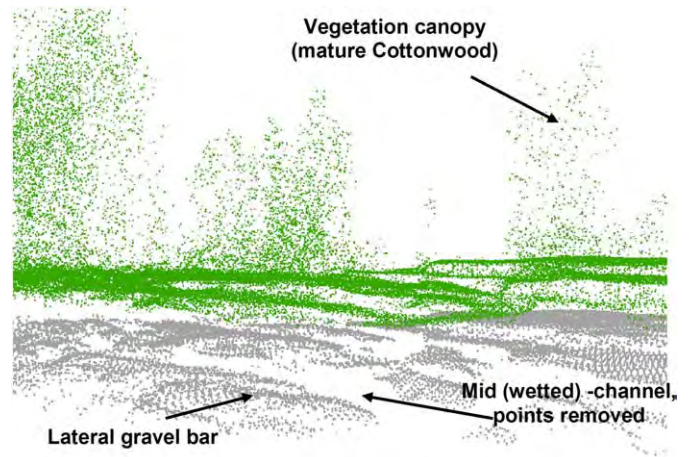


Fig. 3. A LiDAR point cloud of a reach of the Naches River. Point clouds can be defined and classified by hydrogeomorphic feature of surface type enabling the analyst to iteratively improve point classification and, ultimately, surface characterization.

LiDAR points, heighted-breaklines of channel banks and other critical hydraulic structures, such as levees, derived from analysis of stereo imagery using softcopy photogrammetry (Leica Photogrammetry Suite). Some of these structures were well represented by LiDAR points, while some areas clearly required augmenting. To deal with the subaqueous data gap, dense cross-sectional points of the channel and thalweg were also incorporated. Some of these were used to train an isolated multispectral image of the wetted channel using Leica ERDAS image processing software to develop an estimate of bathymetry which can be represented by contours. In our experience this is an unreliable method due to the heterogeneity of spectral return from a gravel-bed river, which is not consistently a function of depth but more likely multiple factors including sun angle, substrate type and caliber, and turbidity. Turbulence is most influential, and causes unpredictable returns. However, enough researchers have utilized this approach to consider it an acceptable technique (Milton et al., 1995; Winterbottom and Gilvear, 1997; Marcus et al., 2003; Leckie et al., 2005) and is applied here to guide an 'expert' approach to bathymetric determination in our study reach. The uncertainties in image (spectral) classification also precluded use of the photogrammetric stereo model of the channel to extract depth measurements using the method reported by Westaway et al. (2003). Approximate depth contours were thus developed using imagery alone, and overlaid on the imagery together with field survey data (cross-sections) and LiDAR elevation points, the latter which fall hard against the river edge in most places (Fig. 5). Fig. 5 illustrates all of this data combined in a GIS environment. This information was sufficient to reliably interpolate a high resolution channel bed and floodplain surface model (SM1), and this visualization environment was used to further develop enough points to develop a second, scenario-realistic surface model (SM2) to simulate (i) bed aggradation, and (ii) channel damming at a site prone to LWD build up. Abbe and Montgomery

Table 2
Data employed in this research.

Data type	Data description	Spatial resolution	Source
LiDAR DTM	Bare earth point cloud augmented with channel bank and other breaklines to gridded DTM	2 m	Collected in 'steward' fashion by Horizons Inc.
Aerial Photography	Color infra-red (CIR) digital dataset (co-flown with LiDAR mission) True color stereo pairs	30 cm pixels 1:10,000 scanned from original negatives at 12.5 µm.	Horizons Inc. US Bureau of Reclamation (Upper Columbia Basin)
Quickbird Satellite Imagery	Panchromatic and Multispectral bands	60 cm (PAN); 2.4 m (XS)	Digital Globe
Channel cross-sections	Multiple densely spaced cross sections (xyz points) describing channel geometry and key breaks in slope	2–15 m spacing	Field survey

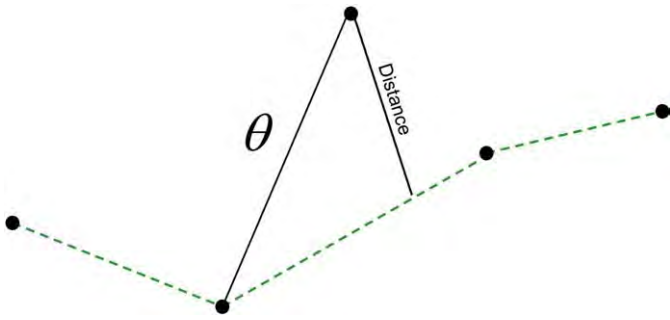


Fig. 4. Iteration parameters determine how close a point must be to a TIN facet plane for that point to be incorporated into the surface model.

(2003) observe that vertical fluctuations in channel elevation are generally equivalent to at least a rootwad diameter, or 2–3 basal diameters of mature riparian trees (a rootwad is a trunk of a tree with the roots attached, and the soil removed so that the roots are exposed). Likewise, up to 2 m of initial vertical aggradation is likely to occur in forested/riparian buffered rivers where snags and log jams form, thus we artificially raised the bed by 2 m in our study area to simulate aggradation behind a LWD jam at a location where field work and aerial photograph analysis indicates this commonly occurs.

Once the data were assembled, the two surfaces were created as a TIN using breaklines as appropriate, with expert points added to the first model, and expert and simulation points added to the second. Error analysis involved comparison of dense field surveyed cross-sections with those cut from the DTM. This involved both a visual comparison of surface fidelity, and a quantitative spatial analysis based on comparison of the difference between total station point elevations and the corresponding elevation value of the constructed surface. This enabled comparison of thousands of points with each raw and bare earth terrain surface developed from the LiDAR (and at various resolutions), and also the registration of deviance with

computed slope angle, this enabling examination of the error field in a spatial context.

The DTM resolution used for this study was 2 m. Multiple, pilot surface representations were generated at 1 m, 1.5 m, 2 m and 3 m by interpolation of sub-sets of mass LiDAR points and breaklines in critical areas (channel and banks). These were then tested for surface fidelity using the techniques described above. 2 m was found to be the optimal cell size enabling generation of cross-sections comparable to those collected in the field (Aggett, 2005) while minimizing computational demand.

4.2. Hydraulic modeling

4.2.1. HEC-GeoRAS (GIS) preprocessing

Geometry set-up in HEC-GeoRAS involved digitizing the stream centerline, predicted overbank flowlines, levees, and a polygon coverage delineating roughness cover. This exercise was facilitated by visual interpretation of the DTM and CIR imagery via 3D fly-through of the river system, and comparison of channel and floodplain cover with estimates of roughness characteristics of the channel using Hicks and Mason (1998) and the floodplain. Finally, very densely spaced (<50 m) cross-sections were digitized ensuring these were kept as perpendicular to flow as possible. Because the primary channel meanders across the active gravel channel frequently changing direction, placement of section lines takes a considerable effort as HEC-RAS requires cross-sections do not overlap at any location. Channel and cross-section lines are then encoded with z values from a TIN surface, a process that was repeated for two sets of data, one lying over SM1, the other over SM2. Once complete, both sets of pre-processed geometry data were exported to HEC-RAS.

4.2.1.1. Modeling in HEC-RAS. Initially a HEC-RAS model was set up with 585 densely spaced cross-sections to provide the channel width and floodplain bed elevations for the study reaches surveyed by Aggett (2005). The HEC-RAS user's manual (US Army Corps of Engineers, 2003) indicates that carefully designated flow subdivisions

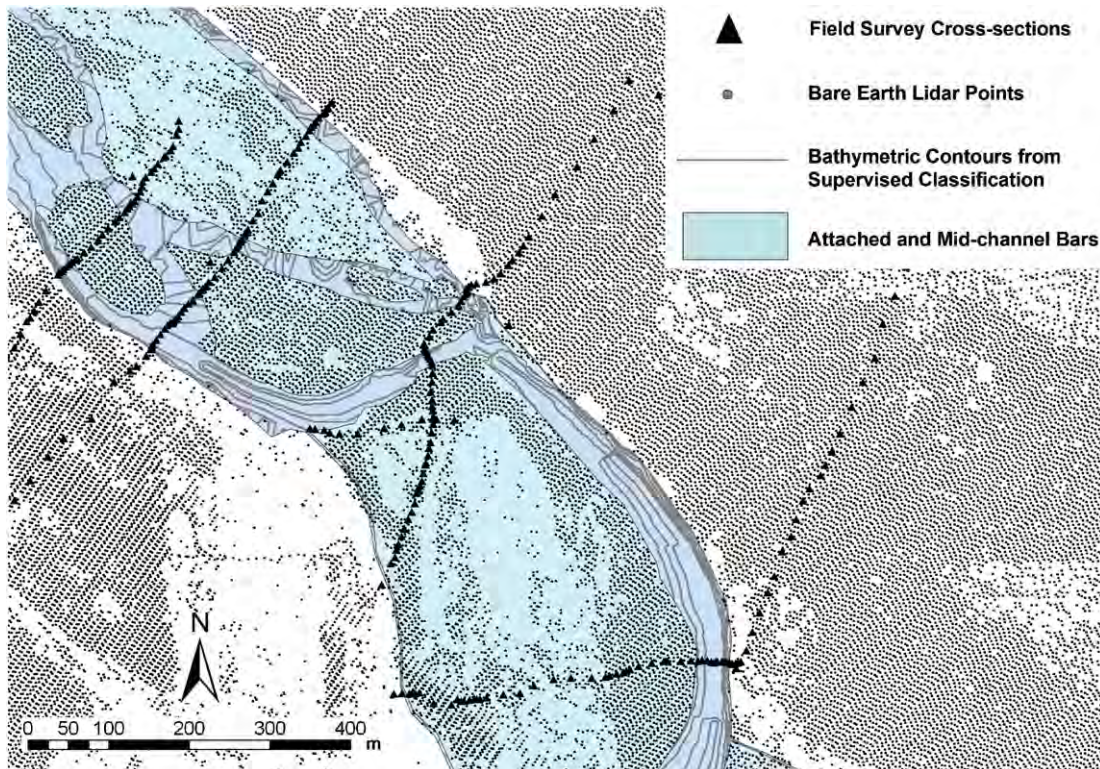


Fig. 5. Data gap modeling approach. Points (x,y,z) along detailed cross-sections were used to train a spectral classification of channel bathymetry using multispectral imagery. Elevation points were extracted from the resulting contours to assist fill the data gap in the wetted part of the channel where no LiDAR data was collected.

(slices) are better than the standard (left and right overbank, channel) subdivision, and our aim was to optimally select these subdivisions based on an assessment of the geometry and n values of the active channel, the ultimate goal being to enhance HEC-RAS performance.

As suggested by the user's manual, a first model run needs to validate model set up using measured or remotely sensed data. To do this, boundary conditions for an initial run were imposed as a dynamic discharge (based on the February 1996 stage recording) at the upstream end of the reach, and an imposed downstream water surface elevation provided by aerial photos taken shortly after the flood crest (6 h) of this rain-on-snow event, which in most locations removed snow up to the edges of flow inundation. At least two sections provided a reasonable boundary with which to interpolate across the LiDAR DTM to gain the water surface height in the channel using a real base elevation obtained from field survey. Notwithstanding geomorphic change in the intervening period (1996–2001), and that utilization of a free surface elevation at the downstream end means that boundary conditions and validation data (including travel time) are not fully independent, the impact of these was found to be negligible.

Following validation, the model was adjusted and rerun for the shorter study reach (62 cross-sections – 3.2 km). Multiple HEC-RAS scenario 'plan' runs were modeled, simulating: (i) the 1996 flood event ($592.5 \text{ m}^3/\text{s}$); (ii) the 1933 (100 yr) flood ($911.8 \text{ m}^3/\text{s}$); and (iii) the US Army Corps of Engineers (1972) predicted 'standard project flood' of $2265 \text{ m}^3/\text{s}^{-1}$ the upper-level event. These were all run using both SM1 and SM2 geometries for the scenario flood event. A number of smaller flow events were also simulated to assess the hydraulic model under non-flood conditions.

Free water surfaces and predicted cross-sectional inundations (Fig. 6), water surface slopes and cross-sectional shear stress and stream power were output for all runs, the latter two attributed to cross-sections in the GIS database for later validation of spatially distributed τ and ω . Inundation and velocity data were exported to HEC-GeoRAS for post-processing.

4.2.2. HEC-GeoRAS (GIS) Post-processing

Predicted inundation extent was derived by exporting the HEC-RAS output water surface back to HEC-GeoRAS, where the water surface was overlaid on the 1996 data, showing excellent correspondence with the flood inundation delineated by snow removal (Fig. 7).

Once in GeoRAS, inundation data for each modeled scenario were converted into a TIN and then a GRID surface. Velocity data were

exported to GeoRAS in point format, each point representing estimated velocity at each cross-section slice. These were also interpolated to a TIN, and then vertices converted to a GRID form and overlaid onto their respective terrain surfaces for careful checking of validity.

Tools exist in HEC-RAS that can be used to simulate raising-lowering of bed level and simulation of damming. These were explored and evaluated to determine if they are more or less effective than the terrain modeling approach when utilizing high resolution (z) geometry.

4.3. Shear stress and stream power modeling

To calculate shear stress, τ , and specific stream power per unit bed area, ω , for our modeled scenarios, we utilized the Spatial Analyst tools in ArcGIS. Recalling Eqs. (1) and (2), critical data layers are channel and floodplain slope, inundation depth, and flow velocity. These GRIDS, being co-located and of the same resolution, were available for cell-based computation of τ and ω (Fig. 8). In locations where grids contained spurious or null data, no calculation was made, this creating a NODATA cell. Once stream power was computed for each scenario, the resulting GRIDS were overlain on top of the terrain model and/or imagery for validation and analysis. Initial assessments utilized hydro-geomorphic units (pools, riffles, glides) classified in a remote sensing study (Aggett, 2005) to assess whether stream power predictions made sense in terms of the expected hydraulics in these units. Although dependant data, the cross-sectional estimates of shear stress and stream power from HEC-RAS provided a useful means to flag data deficiencies in the contributing GRIDS.

5. Terrain model validity

Initial visual interpretation of the DTM (SM1) indicated that there were no obvious spurious defects in the surface (e.g. pits or spikes). By overlaying previously surveyed GIS data (Aggett, 2005) we were able to assess that the wetted channel bed appeared to have been sensibly surfaced in that deeper areas corresponded with pool polygons, steeper flatter sections with riffles. Table 3 provides a comparison of the RMSE (root mean square error) of raw LiDAR points with the RMSE of the computed TIN for the bare earth SM1 DTM. RMSE's were comparable for the asphalt surface which provides a useful control for baseline quality as LiDAR returns should be consistent here, and no post-processing or ancillary data influences the final interpolated

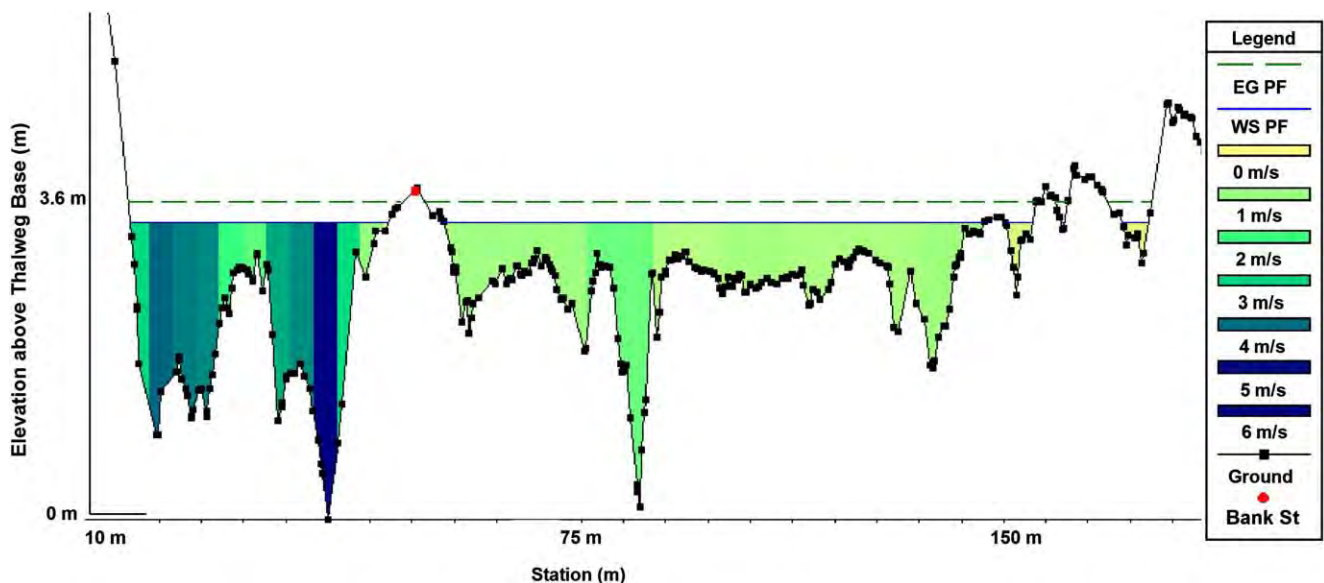


Fig. 6. A sample HEC-RAS cross-section illustrating user-defined bed 'slices' from which velocities are predicted.

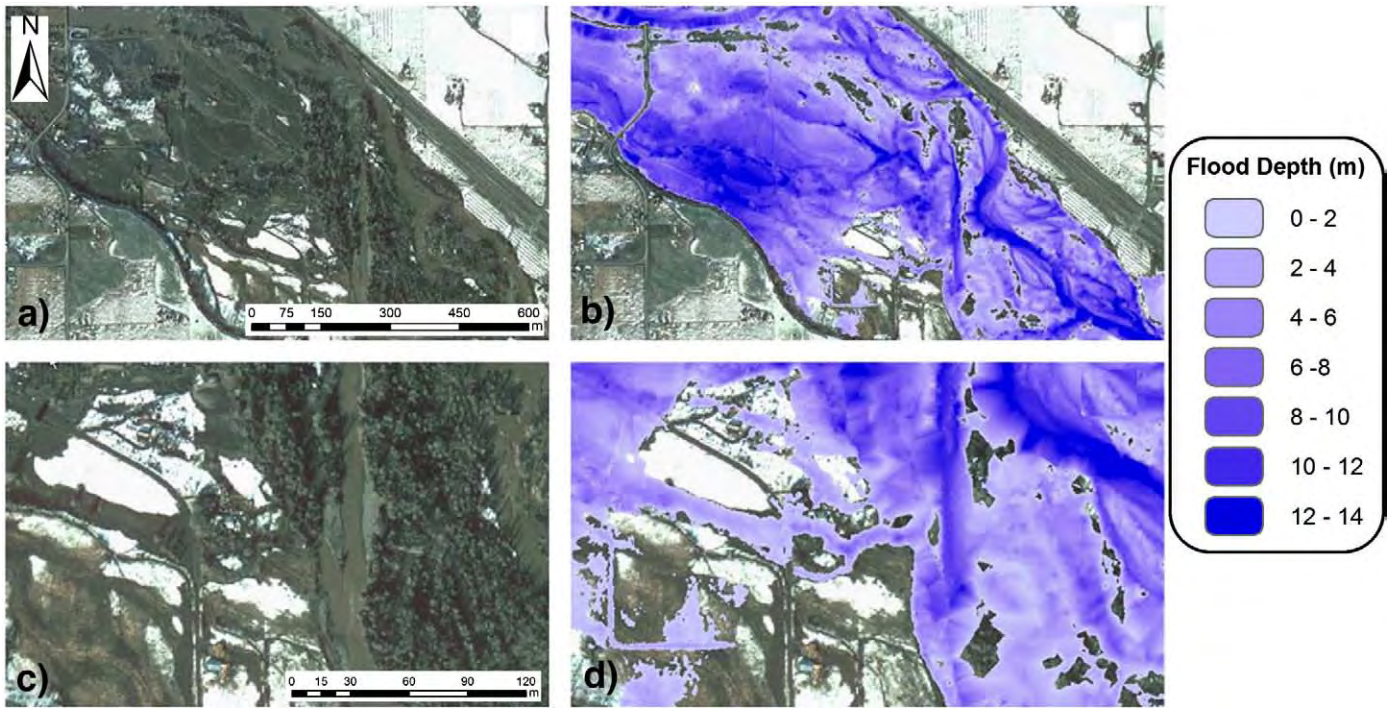


Fig. 7. Inundation surface for modeled 1996 flood (b and d). Predicted surface corresponds well with snow eroded by flood peak flow (a, and c). The ability of the hydraulic model to resolve the detailed topography is illustrated well in (c), where water is flowing along the artificial channel created by a farm track. Darker blue indicates greater flow depth.

surface. The $RMSE_{\text{Observed TIN surface}}$ is remarkably low given the high curvature of bar surfaces.

Evaluation of the broader floodplain surface indicated that highest RMS errors could be expected on steeper slopes, where horizontal error is more influential (Fowler, 2001; Hodgson and Bresnahan, 2004). As these are well outside the 100-year floodplain for our study reach the impacts of this are negligible, but do demonstrate that input of heightened breaklines at channel banks are critical when LiDAR post spacing is greater than about 0.3 m, the density required to capture appropriate information on sudden breaks in slope.

6. Results and map outputs from scenario modeling

6.1. Inundation

Inundation and mapping of flow depth provide a first-order assessment of the potential for a modeled discharge to initiate avulsion, as

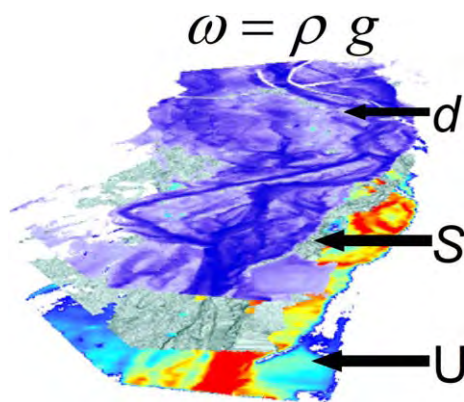


Fig. 8. Stream power methodology. GIS enables spatially distributed data products from hydraulic and terrain modeling to be combined (depth, d , water surface or channel slope, S , and velocity, U), and stream power to be computed for each cell (ρ = density of water, while g = is the gravitational acceleration).

without finding and inhabiting alternative flow lines there is no condition for a change of channel. Fig. 7 indicated the predicted flood surface to be reliable. Combining a predicted water surface with the high resolution terrain model for visualization provides a highly effective means of assessing the potential of a modeled flow to occupy secondary and paleo-channels and to spatially query depths of inundation.

6.2. Shear stress

Sediment transport capacity is related to bed shear stress (Wilkinson et al., 2004), thus a spatially explicit representation of shear stress (τ) provides opportunities to define likely locales of erosion during flood events, both in and out of the main channel. Fig. 9 illustrates modeled shear stress during a 1933-type flood event using both scenarios (SM1 and SM2 model set-up). In this high flow condition it is not surprising we see high values of τ in the main channel against the highway, as the primary channel collides with this reinforced bank section (Fig. 9a). This reach has been noted as a high energy section (Aggett, 2005), and analysis of the LiDAR DTM indicated that prior to 1927 (the historical aerial photographic record of channel change) the channel has aggressively migrated across the current location of Highway 12 at this location. There is also an extreme high shear stress condition on the next meander bend, which has a high curvature containing a deeply scour-channelled lateral bar. This meander comes within 25 m of the secondary channel under investigation for avulsion potential in this paper, and based on the SM1-1933 flood scenario, is identified as a major AHZ.

Table 3
RMSE (m) of raw LiDAR points with the RMSE of the computed TIN for SM1 DTM.

	Land cover type			
	Bare gravel	Low scrub/ grass	Cottonwood (mature)	Asphalt
$RMSE_{\text{Observed LiDAR points}}$	0.193	0.215	0.258	0.176
$RMSE_{\text{Observed in TIN surface}}$	0.332	0.285	0.379	0.212

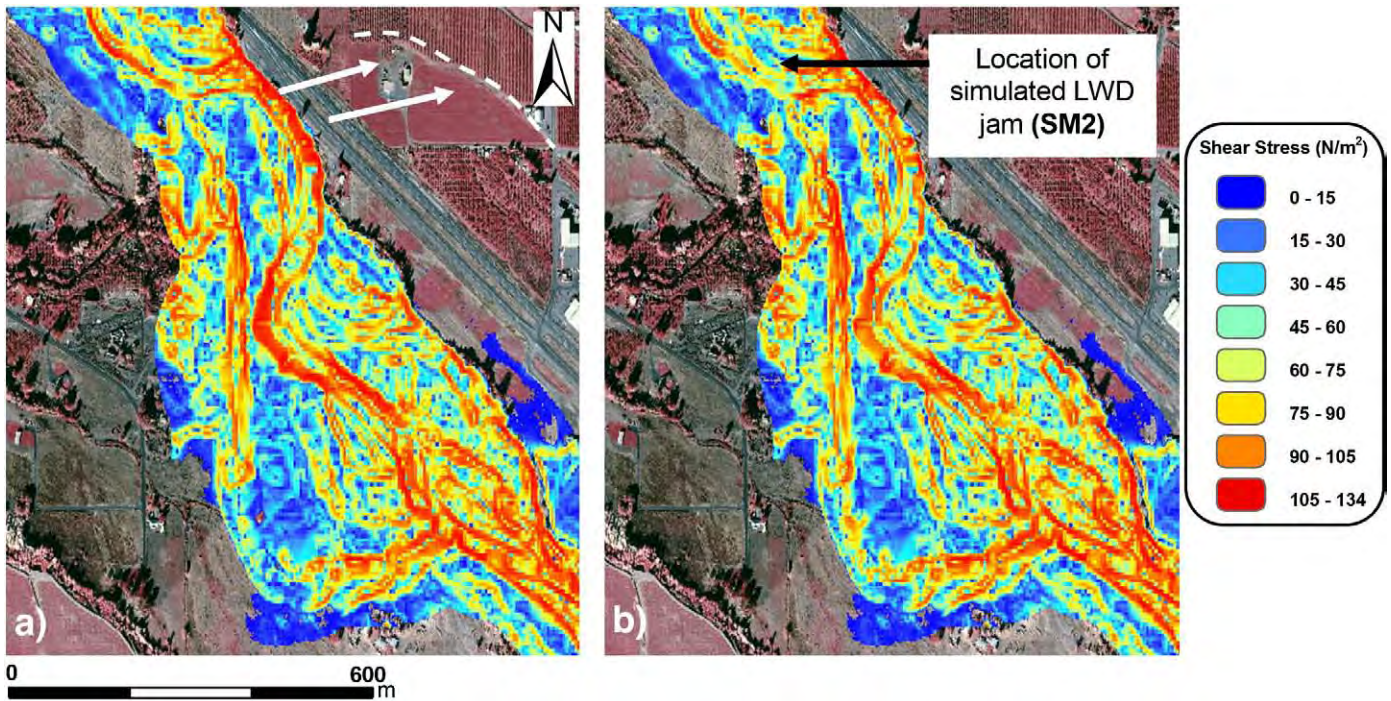


Fig. 9. Shear stress computed for 1933 ($911.8 \text{ m}^3/\text{s}$) scenario flow event using SM1 (a), and SM2 (b) scenarios.

The switch to SM2-1993 conditions (Fig. 9b) creates some notable differences in the spatial distribution of shear stress. Firstly, because more water flows into the secondary channel and less through the primary channel due to LWD jam, one can observe a transfer in relative levels of τ between the primary and relict channel, and considerably higher intensity of τ throughout the length of the relict channel than under SM1-1993 conditions, indicating this flow could facilitate creation of a new primary channel. Key to this is the increase in τ at the lower (southern end) of the relict channel, which field investigation revealed has in-filled and leveled during and following previous flood events, and would require significant sediment transport to scour open a new active channel. The scenario change also indicates substantial change in overbank distribution of τ , especially in the floodplain flanking the relict channel. Where overbank flows have similar τ values as the existing active channel, it is reasonable to assume that there is considerable likelihood of sediment mobilization here.

Upstream of the simulated LWD dam at, aggradation has raised and leveled the bed profile (also simulated), reflected in reduced τ along this sub-reach.

τ requires just inundation depth and slope at a cell to compute its value. Most studies utilizing DTMs to compute stream power have not utilized high-resolution (<5 m) river channel and floodplain DTMs to derive slope. As this research was believed to be novel work we thought it useful to compare stream power computed from our 2 m DTM with that from a USGS 30 m DTM, using the same water depth computed for the 1933 event (SM1). The relative resolution of DTM's is clearly important in reliable prediction of shear stresses in the active channel area (Fig. 10). The derived 30 m slope GRID misses the finer scale breaks in slope signifying critical changes in process-driving gradients representing, for example, pool-riffle sequences and steep scour channels through which flow accelerates. Additionally, in several places the depth (and hence slope) of the primary channel below its surrounding floodplain is not reliably reflected by the data, resulting in discontinuities and some anomalies in the expected spatial structure of computed shear stress. If the USGS (30 m), rather than the LiDAR (2 m) DTM had been used to produce the water depth GRID, computation and spatial representation of τ would have been far more generalized.

6.3. Velocity and stream power modeling

Stream power per unit bed area, ω , is the product of shear stress, τ (determined in Section 5), and flow velocity, U . Considerable attention was thus paid to optimizing HEC-RAS parameterization for computing velocity and creating a surface from the points in GIS. While there are no ground-truth data for this experiment, predicted velocities were within the ranges computed by the US Army Corps of Engineers (1972) for the modelled intermediate (100 yr) Naches River flood ($910 \text{ m}^3/\text{s}$) – 3.7–4.6 m/s in the main (active) channel and 1.5–2 m/s overbank.

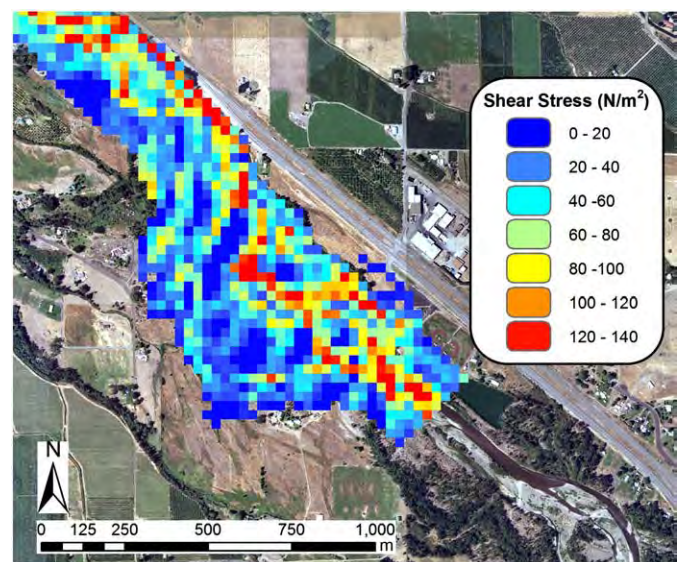


Fig. 10. Shear stress computed using a USGS 30 m DEM for the same 1933 flood event. The coarse nature of the elevation data from which slope is derived means that slope is considerably generalized, significantly influencing computation of shear stress as well as producing output that is not readily interpreted in the context of detailed river morphology.

Fig. 11 presents stream power for 3 scenario discharge events, the 1996 flood, a 100 yr (1933) flood, and the predicted (US Army Corps of Engineers, 1972) upper-level flood event, run using geometry extracted from SM1 (Fig. 11a, b, c), and then SM2 (Fig. 11d, e, f).

Fig. 11a indicates that under the simulated 1996 flow condition, stream power is high in the primary channel (maximum 610 W/m^2) on the outside of the two major meanders, and highest where the channel constricts as it leaves the study area. The potential for work is

very high against the freeway, and against the narrow section of floodplain between the primary and relict channel, which is itself inundated and undergoing considerable geomorphic work in its steep, straight, central reach. Note that ω is dampened where the flow enters the relict channel from the primary channel indicating that some energy is dissipated (flow reduced) in the primary channel where this occurs, and that ω is negligible in the tight meander at the lower end of the reach where the relict channel turns towards the

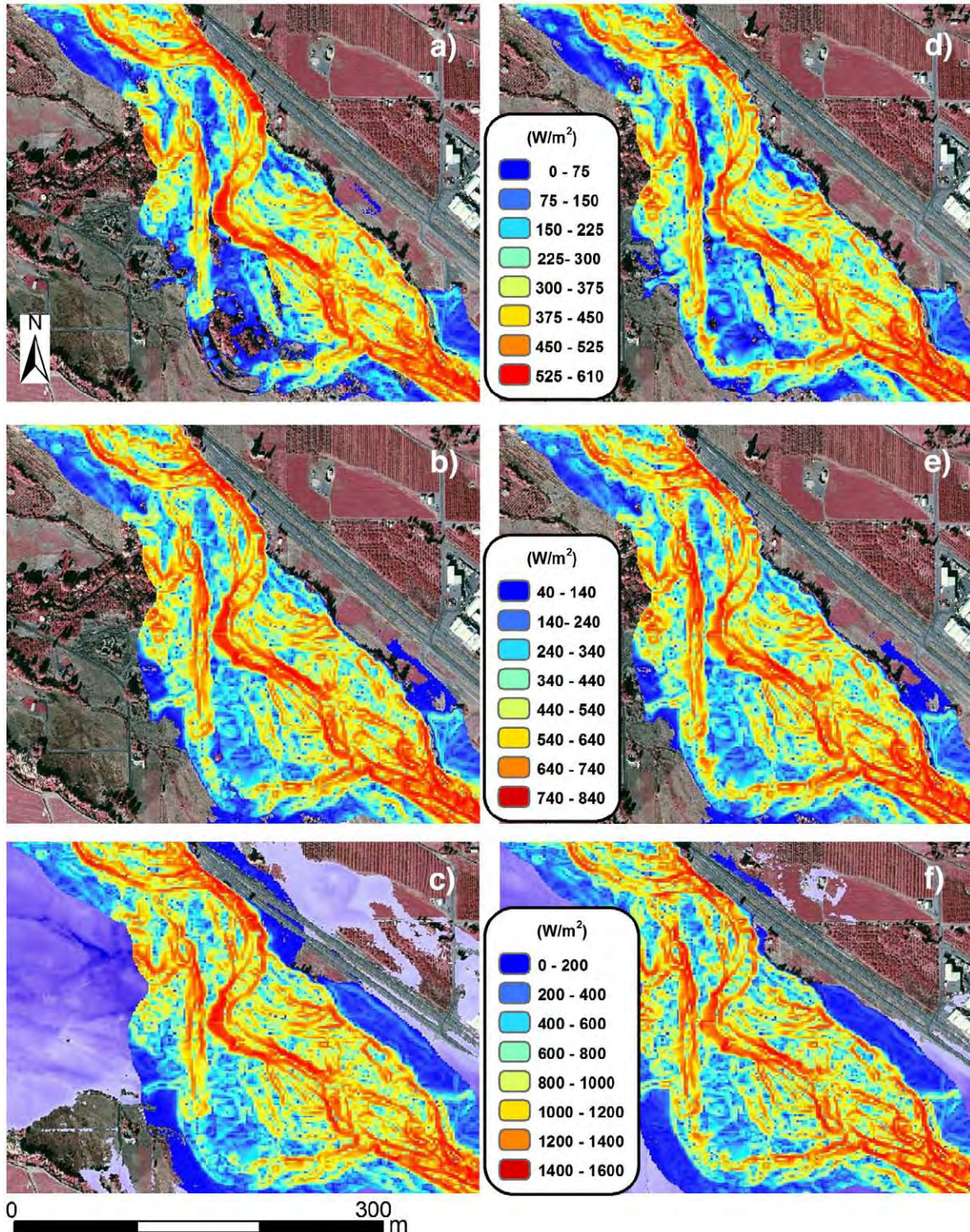


Fig. 11. Predicted specific stream power (ω , W/m^2) for three flood scenarios using SM1 and SM2 geometries. (a): 1996-SM1; (d): 1996-SM2. (b): 1933-SM1; (e): 1933-SM2. (c): 'standard-project'-SM1; (f): 'standard-project'-SM2. Note that scales of ω (W/m^2) vary for each flood.

primary channel. This is because the gradient is flat here due to infilling from fluvial deposition and mass-wasting of the steep banks on the lower end of the channel. In the SM2 scenario (Fig. 11d) ω rises in this area as a considerable volume of flow is diverted into the relict channel due to LWD damming. The impact of this in the relict channel is clear as ω rises along its course and flanking overbank areas. As levels of predicted stream power begin to approach that of the main active channel, similar degrees of geomorphic work are being done, and at a channel forming level. Hence we could expect channel switching to occur if this degree of work is maintained. The increase in work done in the relict channel corresponds with an expected decrease in the primary channel in this SM2 scenario. However, the relatively high levels of geomorphic work being done in both channels at the narrow gap of floodplain between them points to the potential for the river to punch through here to connect the channels.

The 100 yr flood (1933, SM1 scenario – Fig. 11b) begins to produce stream powers in the relict channel the highest of which are comparable with the lowest in the main channel (530 W/m^2). While noticeable in contrast to the 1996 scenario, levels of work in the lower reach and meander of the relict channel are relatively small even compared to areas of the floodplain, thus we might not expect to see the infill material removed rapidly. This condition changes under SM2 conditions however. Stream power rises on the meander bend and through the dog-leg reach of the relict channel to its confluence with the primary channel. This scenario is thought to have potential for the flood flow to transport and carve into the relatively low caliber infill material, and steepen the gradient of this section of the relict channel, generally enhancing hydraulic conditions for avulsion into the relict channel.

The more improbable 'standard project flood' of 2265 m/s^3 produced very high ω values in excess of 1400 W/m^2 in the primary channel (SM1), 1150 W/m^2 in the relict channel (SM2), and 750 W/m^2 in parts of the active channel floodplain. Inundation GRIDs have been co-displayed under the stream power data to highlight the distribution of flood extent under the two scenario conditions. In SM1 (Fig. 11c), the flood crosses Highway 12 and covers the freeway from the lower right of this image downstream. In SM2 (Fig. 11f), we observe less water filling the freeway intermedian, having been redistributed to the other side of the floodplain. This highlights the importance this type of scenario modeling has for better understanding of flood hazard, as well as geomorphic processes.

Fig. 11a indicates that the ability for the flood flow to do geomorphic work in this scenario is negligible on the meander bend of the relict channel. For avulsion to occur through this part of the floodplain, flow would have to scour enough material to clear the infill accumulated in this area and to create a graded channel. The actual 1996 flood did not succeed in doing this, and the meander bend is now a ponded backwater channel. Fig. 11b, c indicates that under these flood conditions (SM1), stream power steadily increases in the secondary channel under increasing flows. Thus there exists considerably greater avulsion potential in the larger two of the three events, whereas in the simulated debris dam and aggradation scenario, we see a considerable switching of stream power from the primary channel to the secondary channel even under the relatively modest 1996 flood condition (Fig. 11d).

7. Discussion

7.1. Terrain modeling

Dense elevation data and new geospatial tools for creating detailed digital terrain models of the channel and floodplain are becoming widespread, and encouraging novel methods to get past the limitations of these data (e.g. the data gap in the wetted channel) to create surfaces valid for hydraulic modeling. The ability to quite rapidly adjust a surface using precisely placed heighted elevation points and lines, once the

described data inputs are set up in the terrain modeling environment, enables an infinite number of adjustments to be made including construction (or removal) of structures such as dams, levees and LWD assemblages. The ability to check such a surface by visualizing and measuring specific features in great detail provides the confidence necessary to proceed with hydraulic modeling. Such an environment paves the way for the scenario modeling presented here, and provides significant advantages over tools in models such as HEC-RAS to model features such as levees, and complications such as ice-jams and bed aggradation. The limitation with the latter function in HEC-RAS, as compared to the terrain modeling approach developed here, is that simulated sediment deposition occurs only along the width of the defined primary channel, rather than spread across the active channel in a lens that more realistically reflects deposition in a wide active gravel-bed river.

There are few guidelines in the geomorphology literature for the selection of an appropriate DTM cell size to interpolate LiDAR mass points, based on, for example, the average LiDAR point density per m^2 (following removal of points to generate the bare-earth dataset described above). This is likely because: (i) LiDAR datasets from different vendors have variable post spacing and point densities, (ii) vegetative conditions and post processing methods to remove vegetation will yield different point densities (see Fig. 5 – note the bare areas where riparian and bar vegetation was dense and has resulted in sparse ground sampling by the LiDAR sensor), and (iii) analysts may have at their disposal ancillary data, such as the bank breakline data generated to support this work, which might allow for locally improved representation of terrain. For geomorphologic applications we recommend that LiDAR mass points and associated data such as breaklines be maintained as a raw DSM (digital surface model) allowing for manipulation of the data per project requirements. For example, a subset of points and breaklines can be extracted from the DSM and possibly augmented by detailed field survey points to generate a 0.2 m DTM for bank erosion modeling, while another study might have more general flow routing requirements that only require a 5 m DTM.

7.2. Hydraulic modeling with HEC-RAS

Selection of HEC-RAS for this project was based on its widespread application and relative ease of use. In the context of 2-D models, Hardy et al. (1999) have argued that the spatial resolution at which a model is applied affects the solution of the equations and thus the simulation results. This assumption was made here for the 1D case, with the expectation that enhanced parameterization of model geometry can enhance HEC-RAS outputs. Bates et al. (2003) have recently identified this as an emergent research area – how to integrate massive (topographic) datasets with lower resolution numerical inundation models in an optimum manner that makes maximum use of the information content available.

We thus proceeded to optimize HEC-RAS performance by developing and utilizing the LiDAR-based terrain model to characterize geometry with detailed cross-sections, optimally spaced and oriented to capture the hydraulic influence of this parameter. In addition, we utilized a data and visualization rich environment to select optimal n values for in-channel and overbank cross-section 'slices'. With the model calibrated to existing hydrometric data (1996 flood), this effort resulted in excellent predictions of inundation. While it is unclear whether a parameter set calibrated against data from an event of a certain magnitude will be valid for a more extreme event (e.g. Horritt and Bates, 2002), we nonetheless proceeded with some faith that the initial model setup was performing realistically.

Key to this optimization effort was the employment of the GIS-based GeoRAS pre- and post-processor. This hydraulic model-GIS integration greatly facilitates modeling efforts by allowing development of geometry and other parameters such as n values to be developed in a fully spatial ('real-world') setting, where cross-sections can be deployed

and later refined based on interpretation of detailed terrain and image data. Model geometry development can be achieved relatively quickly (notwithstanding the issue of ensuring cross-sections do not overlap), and imported into HEC-RAS for flow calculations. Results from hydraulic analysis can then be exported back into GIS and reprojected on to the detailed LiDAR-based terrain surface to establish floodplain extent and evaluate flood depth.

Transfer of velocity data between HEC-RAS and GIS is more complicated. Water velocities can vary considerably in between cross sections, depending on the changing channel geometry. To establish water velocities, GeorAS employs velocity points on the cross sections as mass points, and the cross sections as breaklines to create a velocity TIN. GeorAS then sets velocities to zero in cells with water depth values of zero, eliminating an obvious potential interpolation error. This worked very well where the hydraulic model has densely located cross sections and a gradually varying channel shape. However, it tended to break down inexplicably in less homogenous zones, despite having performed well in similarly complex regions elsewhere (Fig. 12). Refinement of geometry would often fix the problem (usually densification of cross-sections and subtle re-orientation), only to have a similar breakdown elsewhere. Because of the dense spacing of cross-sections, re-orientation of one cross-section would always impact on two or more other sections which would also need re-orienting, this consuming a large amount of modeling resources. This was somewhat offset by data transfer between HEC-RAS and GIS via GeorAS being reasonably efficient, enabling rapid visualization of results and hence opportunities for model diagnostics. Implausible velocity distributions were most often assessed to be due to flaws in model setup (i.e. channel data were not adequately refined to support velocity distribution calculations), an observation supported by continual refinement and subsequent improvement in results.

Geometry and roughness most likely have the greatest impact on inundation prediction and flow characteristics in hydraulic modeling. Parameterization of HEC-RAS with such densely spaced and detailed geometry (a new approach in 1D modeling) thus requires more focused investigations into the impact this type of surface can have on model performance. Pappenberger et al. (2005) recently conducted an uncertainty analysis of the unsteady flow component (UNET) of HEC-RAS using the generalized likelihood uncertainty estimation (GLUE). This Monte Carlo method allows that different parameter sets within a model structure (in their case roughness) might perform equally well in reproducing the limited field observations in any practical application. GLUE accounts for this by running the model with many randomly

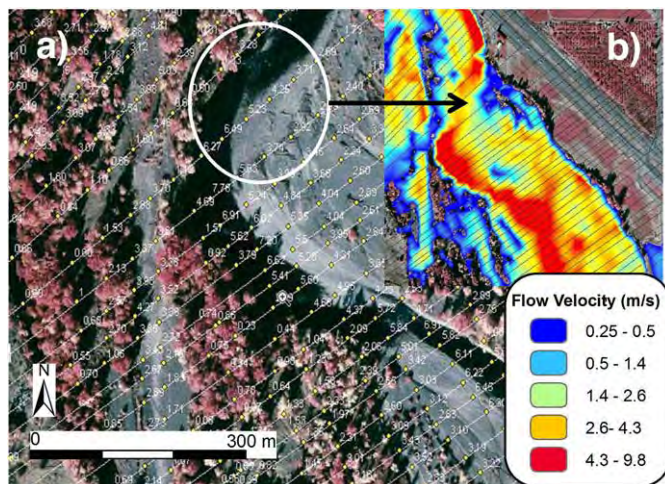


Fig. 12. Geometry (a) and predicted flow velocities (b) for cross-sectional 'slices' for an example HEC-RAS model set-up. Note density of cross-sections, with slightly wider spacing at the circle marker. This greater spacing and/or orientation with the section line not perpendicular to flow caused a poor estimation of velocities over this riffle, requiring a re-set of model geometry.

chosen sets of parameters. This type of parameter assessment is likely to lead to a better understanding, and ultimately use, of high resolution DTM's in 1D hydraulic modeling.

7.3. Shear stress and stream power modeling

Flow and flood surface modeling under pre-existing and future (predicted) scenario conditions is clearly helpful in understanding avulsion potential. However, inundation alone does not imply avulsion will occur. Flows need to be powerful and sustained enough to create opportunities for a new flow line to become the preferred direction, a condition that implies some geomorphic work must be done.

Modeling and visualization of detailed and spatially distributed estimates of shear stress and stream power under scenario conditions can facilitate more confident delineation of the avulsion hazard zone, and also create the potential to develop a probabilistic estimate of this hazard based on flood return periods. Stochastic elements such as LWD damming and channel aggradation may be built into this modeling approach. Wood debris is a major geomorphic agent in forested regions, and an important influence on avulsion, thus fluvial geomorphic modeling needs to account for its influence in spite of the challenges (Montgomery and Piegay, 2003), and the methods presented here are one attempt at this.

A key advantage of the high-resolution terrain modeling and GIS-based approach put forward here is that outputs of spatially explicit stream power can be related to other spatial data on hydraulic structures such as dams and levees, and used to assess management impacts. For example, in assessing the CMZ of the Naches River, Aggett (2005) has suggested removal of levees on the west side of the river to reduce erosive pressure on a water treatment facility located on a lateral bar on the east side (4.5 km downstream from the avulsion study site). Currently both sides of the channel are narrowly constrained by rip-rap, creating super-critical flows in flood discharges. Buy-out of a few farm properties on the western side could allow several km² of floodplain to be reactivated (a major highway runs the east-side). Modeling of energy redistribution under likely flood flows provides a convincing argument for this option.

As well as contributing to avulsion hazards, LWD is also recognized as a key component of the riverine ecosystem (e.g. Crispin et al., 1993). Engineered log jams (ELJs) are now increasingly being installed on river systems to mimic the effects of naturally accumulating LWD, including habitat enhancement, directing flows away from stream banks to prevent erosion, and providing grade control to retain sediment and provide bank stabilization by dissipating flow energy. Selecting the type of ELJ and best location to install it in a restoration project depends partly on the physical characteristics of the river. Scenario evaluation of the impact of ELJs on river hydraulics could be used to assess the potential effectiveness of these features prior to their construction.

The method presented here enables calculation of spatially explicit τ and ω at a point in time (peak of the modeled flood hydrograph). Modeling of the temporal as well as spatial variability of τ during a flood event would add considerably to predictions of avulsion potential, indicating the duration of work being done. Modeling of both spatial and temporal variability of ω for a larger reach would provide opportunities for the fluvial geomorphologist to relate these modeled physical processes with conceptual models of fluvial geomorphology, and to adopt a more spatially explicit approach to evaluation of the influence of stream power on channel change thresholds (e.g. Magilligan, 1992).

Finally, methods presented here offer tools to move towards more spatially explicit processed-based classifications of river channels, an approach advocated by Montgomery and Buffington (1993). In order to sensibly mitigate natural hazards, planners require a spatial understanding of the impact of processes in a probabilistic or deterministic context. Similarly, landuse managers require tools that

identify parts of the landscape in which various level of protection should be applied in order to minimize or prevent environmental degradation of the river system. There are considerable limitations to methods that use increasingly fine-scale spectral data to map similarly fine, but static hydrogeomorphic units to characterize dynamic fluvial systems (the boundaries of which change frequently). More useful is modeling and mapping of various process domains using physical laws and morphologic relationships (e.g. Whiting and Bradley, 1993). While spatially explicit (GIS-based) model predictions have until recently been limited by available DTM cell size, both at the watershed (e.g. Zhang and Montgomery, 1994) and channel scale (e.g. Downs and Priestnall, 1999), advances in high resolution terrain modeling of river channels have advanced our ability to model and map river channel processes in a more spatially detailed manner. Because both shear stress and stream power will be maximized where the depth-slope product is maximized (i.e. zones where either slope or depth increase), spatially explicit scenario modeling of these parameters is dependant on a reliable high spatial resolution (<5 m) DTM to capture variability of stream power at the scale of pool-riffle sequences, and influential changes in slope on the floodplain that may be invisible on a 10 or 30 m DTM.

8. Conclusions

The need to better understand catastrophic river channel change, now recognized to constitute a greater hazard than overbank flow in some areas (FEMA, 1999), is driving new ways to assess contributing processes. Here we coupled HEC-RAS with a detailed LIDAR-based DTM to extend hydraulic model performance and generate scenario-based predictions of inundation and water depths. These assessments are thought to be very reliable based on the quality of the terrain surface, and the degree of model parameterization this afforded. The GIS-based pre- and post-processor facilitated this work, enabling careful selection and digitization of model geometry and n values for input into HEC-RAS, and optimal visualization of the inundation surface projected onto the DTM. Scenario-based inundation maps alone provided significant improvements in our ability to assess and delineate avulsion potential on the Naches River. This scenario approach was strengthened by modifying the DTM to simulate LWD damming and bed aggradation, an influential but poorly understood fluvial process relative to sediment transport. Architectural approaches to terrain modeling of the channel provide opportunities to escape the limitations of 1D fixed bed hydraulic modeling, and to impose (or remove) planned structures on the riverscape.

Given the reliability of the slope and water depth data, surfaces of predicted τ were also thought to be reliable, and provide a useful measurement to couple with spatially distributed data on sediment caliber to estimate the volume of sediment transported on the bed, a focus of ongoing research. Spatially distributed estimates of ω , while being somewhat less reliable due to uncertainties in HEC-RAS velocity output, nonetheless provided visually realistic and sensible mapped output to compare and contrast relative degrees of geomorphic work being done in and out of the primary channel. Given the importance of the AHZ in the CMZ mapping process, this quantitative, spatially explicit information can greatly enhance the reliability of CMZ delineation, and could also be used to assess the potential efficacy of engineered log jam (ELJ) installation in river restoration projects.

References

- Abbe, T.B., Montgomery, D.R., 2003. Patterns and processes of wood debris accumulation in the Queets River Basin, Washington. *Geomorphology* 51, 81–107.
- Aggett, G., 2005. Applying Advanced Geospatial Data and Methods to Monitoring and Modeling Fluvial Processes. Ph.D. Dissertation, University of Southern California, Los Angeles, USA.
- Baker, V.R., Costa, J.E., 1987. Flood power. In: Mayer, L., Nash, D. (Eds.), *Catastrophic Flooding*. Allen and Unwin, London, pp. 1–21.
- Bates, P.D., Anderson, M.G., Horritt, M., 1998. Terrain information in geomorphological models: stability, resolution and sensitivity. In: Lane, S.N., Chandler, J.H., Richards, K.S. (Eds.), *Landform Monitoring, Modelling and Analysis*. Wiley, Chichester, pp. 279–310.
- Bates, P.D., Marks, K.J., Horritt, M.S., 2003. Optimal use of high-resolution topographic data in flood inundation models. *Hydrological Processes* 17, 537–557.
- Bryant, M., Falk, P., Paola, C., 1995. Experimental study of avulsion frequency and rate of deposition. *Geology* 23, 365–369.
- Charlton, M.E., Large, A.R.G., Fuller, I.C., 2003. Application of airborne LIDAR in river environments: the River Coquet, Northumberland, UK. *Earth Surface Processes and Landforms* 28, 299–306.
- Costa, J.E., O'Connor, J.E., 1995. Geomorphically effective floods. In: Costa, J.E., Miller, A.J., Potter, K.W., Wilcock, P. (Eds.), *Natural and Anthropogenic Influences in Fluvial Geomorphology*. Monograph, vol. 89. American Geophysical Union, Washington D.C., pp. 45–56.
- Crispin, V.R., House, D., Roberts, D., 1993. Changes in instream habitat, large woody debris, and salmon habitat after restructuring of a coastal Oregon stream. *North American Journal of Fisheries Management* 13, 96–102.
- Downs, P.W., Priestnall, G., 1999. System design for catchment-scale approaches to studying river channel adjustments using a GIS. *International Journal of Geographical Information Science* 13, 247–266.
- FEMA, 1999. Riverine erosion hazard areas mapping feasibility study. Federal Emergency Management Agency (FEMA).
- Finlayson, D.P., Montgomery, D.R., 2004. Modeling large-scale fluvial erosion in geographic information systems. *Geomorphology* 53, 147–164.
- Fowler, R., 2001. Topographic LiDAR. In: Maune, D.F. (Ed.), *Digital Elevation Model Technologies and Applications: The DEM users manual*. American Society for Photogrammetry and Remote Sensing, Bethesda, Maryland, pp. 207–236.
- French, J.R., 2003. Airborne LIDAR in support of geomorphological and hydraulic modeling. *Earth Surface Processes and Landforms* 28, 321–335.
- Fuller, I.C., Large, A.R.G., Milan, D.J., 2003. Quantifying channel development and sediment transfer following chute cutoff in a wandering gravel-bed river. *Geomorphology* 54, 307–323.
- Grounds, J.S., Anderson, E.L., Meyer, W.B., 2004. Quality control of LiDAR for a flood insurance study. Geographic Information Systems and Water Resources III – AWRA Spring Specialty Conference. AWRA, Nashville, Tennessee.
- Guedet, P., Wells, G., Maidment, D.R., Neuenschwander, A., 2004. Influence of the post-spacing density of the LiDAR-derived DEM on flood modeling. Geographic Information Systems and Water Resources III – AWRA Spring Specialty Conference. AWRA, Nashville, Tennessee.
- Gurnell, A., Montgomery, D., 1998. Hydrological applications of GIS. *Hydrological Processes* 12, 821–822.
- Hardy, R.J., Bates, P.D., Anderson, M.G., 1999. The importance of spatial resolution in hydraulic models for floodplain environments. *Journal of Hydrology* 216, 124–136.
- Haugerud, R.A., Weaver, C.S., Harless, J., 2001. Finding faults with LIDAR in the Puget Lowland. *Seismological Research Letters* 72, 253.
- Heller, P.L., Paola, C.J., 1996. Downstream changes in alluvial architecture: an exploration of controls on channel stacking patterns. *Journal of Sedimentary Research* B 66, 297–306.
- Hicks, D.M., Mason, P.D., 1998. Roughness characteristics of New Zealand rivers. National Institute for Water and Atmospheric Research – Water Resources Publications. LLC, Wellington, NZ. 329 pp.
- Hodgson, M.E., Bresnahan, P., 2004. Accuracy of airborne LiDAR-derived elevation: empirical assessment and error budget. *Photogrammetric Engineering and Remote Sensing* 70, 331–339.
- Horritt, M.S., Bates, P.D., 2002. Evaluation of 1D and 2D numerical models for predicting river flood inundation. *Journal of Hydrology* 268, 87–99.
- Knighton, A.D., 1999. Downstream variation in stream power. *Geomorphology* 29, 293–306.
- Lane, S.N., 1998. The use of digital terrain modelling in the understanding of dynamic river channel systems. In: Lane, S.N., Chandler, J.H., Richards, K.S. (Eds.), *Landform Monitoring, Modelling and Analysis*. Wiley, Chichester, pp. 311–342.
- Lane, S.N., Chandler, J.H., 2003. Editorial: the generation of high quality topographic data for hydrology and geomorphology: new data sources, new applications, and new problems. *Earth Surface Processes and Landforms* 28, 229–230.
- Lane, S.N., Richards, K.S., Chandler, J.H., 1993. Developments in photogrammetry; the geomorphological potential. *Progress in Physical Geography* 17, 306–328.
- Lane, S.N., Chandler, J.H., Richards, K.S., 1994. Developments in monitoring and modelling small-scale river bed topography. *Earth Surface Processes and Landforms* 19, 349–368.
- Lane, S.N., Reid, S.C., Westaway, R.M., Hicks, D.M., 2004. Remotely sensed topographic data for river channel research: the identification, explanation and management of error. In: Kelly, R., Drake, N., Barr, S. (Eds.), *Spatial Modelling of the Terrestrial Environment*. Wiley, Chichester, pp. 113–136.
- Leckie, D.G., Cloney, E., Jay, C., Paradine, D., 2005. Automated mapping of stream features with high-resolution multispectral imagery: an example of the capabilities. *Photogrammetric Engineering and Remote Sensing* 71, 145–155.
- Leys, K.F., Werrity, A., 1999. River channel planform change: software for historical analysis. *Geomorphology* 29, 107–120.
- Lorang, M.S., Aggett, G.R., 2005. Potential sedimentation impacts related to dam removal: Icicle Creek, Washington, USA. *Geomorphology* 71, 182–201.
- Mackey, S.D., Bridge, J.S., 1995. Three dimensional model of alluvial stratigraphy: theory and application. *Journal of Sedimentary Research* B 65, 7–31.
- Magilligan, F.J., 1992. Thresholds and the spatial variability of flood power during extreme floods. *Geomorphology* 5, 373–390.
- Maidment, D. (Ed.), 2002. *Arc Hydro: GIS for Water Resources*. ESRI Press, Redlands, CA. 203 pp.

- Marcus, W.A., Legleiter, C.L., Aspinall, R., Boardman, J.W., Crabtree, R.L., 2003. High resolution hyperspectral mapping of in-stream habitats, depths, and woody debris in mountain streams. *Geomorphology* 55, 363–380.
- Marks, K., Bates, P., 2000. Integration of high-resolution topographic data with floodplain flow models. *Hydrological Processes* 14, 2109–2122.
- Miller, T., 1991. A model of stream channel adjustment: assessment of Rubey's hypothesis. *Journal of Geology* 99, 699–710.
- Milton, E., Gilvear, D.J., Hooper, I., 1995. Investigating changes in fluvial systems using remotely sensed data. In: Gurnell, A., Petts, G.E. (Eds.), *Changing Rivers*. Wiley, Chichester, pp. 277–301.
- Montgomery, D.R., Buffington, J.M., 1993. Channel classification, prediction of channel response, and assessment of channel condition. TFH-SH10-93-002, Washington State Department of Natural Resources.
- Montgomery, D.R., Piegay, H., 2003. Editorial – wood in rivers: interactions with channel morphology and processes. *Geomorphology* 51, 1–5.
- Nicholas, A.P., Walling, D.E., 1998. Numerical modeling of floodplain hydraulics and suspended sediment transport and deposition. *Hydrological Processes* 12, 1339–1355.
- O'Connor, J.E., Jones, M.A., Haluska, T.L., 2003. Flood plain and channel dynamics of the Quinault and Queets Rivers, Washington, USA. *Geomorphology* 51, 31–59.
- Omer, C.R., Nelson, J., Zundel, A.K., 2003. Impact of varied data resolution on hydraulic modeling and floodplain delineation. *Journal of the American Water Resources Association* 39, 467–475.
- Pappenberger, F., Beven, K., Horrit, M., Blazkova, S., 2005. Uncertainty in the calibration of effective roughness parameters in HEC-RAS using inundation and downstream level observations. *Journal of Hydrology* 302, 46–69.
- Raber, G.T., Jensen, J.R., Schill, S.R., Schuckman, K., 2002. Creation of digital terrain models using an adaptive LiDAR vegetation point removal process. *Photogrammetric Engineering and Remote Sensing* 68, 1307–1315.
- Rapp, C.F., Abbe, T.B., 2003. A framework for delineating channel migration zones. #03-06-027, Washington State Department of Ecology, Olympia.
- Rhoads, B.L., 1987. Stream Power Terminology. *Professional Geographer* 39, 189–195.
- Shapiro, M.G., Nelson, E.J., 2004. Digital terrain model processing for integrated hydraulic analysis and floodplain mapping. In: Sehlke, G., Hayes, D.F., Stevens, D.K. (Eds.), *World Water Congress 2004*, Salt Lake City, Utah.
- Springer, G.S., Wohl, E.E., Foster, J.A., Boyer, D.G., 2003. Testing for reach-scale adjustments of hydraulic variables to soluble and insoluble strata: Buckeye Creek and Greenbrier River, West Virginia. *Geomorphology* 56, 201–217.
- US Army Corps of Engineers, SD, 1972. Flood Plain Information – Naches River. Prepared for Yakima County, Yakima.
- US Army Corps of Engineers, H.E.C., 2003. HEC-RAS User Manual. Davis, CA.
- Wang, Y., Zheng, T., 2005. Comparison of light detection and ranging and National Elevation Dataset digital elevation model on floodplains of North Carolina. *Natural Hazards Review* 6, 34–40.
- Westaway, R.M., Lane, S.N., Hicks, D.M., 2000. The development of an automated correction procedure for digital photogrammetry for the study of wide, shallow, gravel bed rivers. *Earth Surface Processes and Landforms* 25, 1–18.
- Westaway, R.M., Lane, S.N., Hicks, D.M., 2003. Remote survey of large-scale braided, gravel-bed rivers using digital photogrammetry and image analysis. *International Journal of Remote Sensing* 24, 795–816.
- Whiting, P.J., Bradley, J.B., 1993. A process-based classification system for headwater streams. *Earth Surface Processes and Landforms* 18, 603–612.
- Wilkinson, S.N., Keller, R.J., Rutherford, I.D., 2004. Phase-shifts in shear stress as an explanation for the maintenance of pool-riffle sequences. *Earth Surface Processes and Landforms* 29, 737–753.
- Winterbottom, S.J., Gilvear, D.J., 1997. Quantification of channel bed morphology on gravel-bed rivers using airborne multispectral imagery and aerial photography. *Regulated Rivers, Research and Management* 13, 489–499.
- Wise, S.M., 1998. The effect of GIS interpolation errors on the use of digital elevation models in geomorphology. In: Lane, S.N., Chandler, J.H., Richards, K.S. (Eds.), *Landform Monitoring, Modelling and Analysis*. Wiley, Chichester, pp. 139–164.
- Zhang, W., Montgomery, D.R., 1994. Digital elevation model grid size, landscape representation, and hydrologic simulations. *Water Resources Research* 30, 1019–1028.